Applied Physics Letters

# Mechanical behavior of ultralight nickel metamaterial

Cite as: Appl. Phys. Lett. **118**, 081902 (2021); https://doi.org/10.1063/5.0031806
Submitted: 23 October 2020 . Accepted: 09 February 2021 . Published Online: 24 February 2021

Pankaj Rajak, Aiichiro Nakano, Priya Vashishta, and Rajiv Kalia









AIP Publishing

Applied Physics Letters ARTICLE scitation.org/journal/apl

# Mechanical behavior of ultralight nickel metamaterial

Cite as: Appl. Phys. Lett. **118**, 081902 (2021); doi: 10.1063/5.0031806
Submitted: 23 October 2020 · Accepted: 9 February 2021 ·
Published Online: 24 February 2021



Pankaj Rajak,[1,2] Aiichiro Nakano,[1] Priya Vashishta,[1] and Rajiv Kalia[1,a)]

## AFFILIATIONS

[1]Collaboratory for Advanced Computing and Simulations, Department of Physics and Astronomy, Department of Computer Science, Department of Chemical Engineering and Materials Science, Department of Biological Sciences, University of Southern California, Los Angeles, California 90089-0242, USA
[2]Argonne Leadership Computing Facility, Argonne National Laboratory, Argonne, IL 60439, USA

[a)]Author to whom correspondence should be addressed: rkalia@usc.edu

## ABSTRACT

The mechanical response of ultralight kagomé structures consisting of hollow nickel (Ni) nanotubes and solid Ni nanorods to compression is studied using molecular dynamics simulations. In both kagomé architectures, $\frac{1}{6}[112]$ Shockley partial dislocations and twin formation are observed under compression. The structure made from solid nanorods shows deformation near both the nodes and beams of the kagomé lattice. The hollow kagomé architecture has a higher yield point than the solid kagomé structure. The deformation in the hollow nanotube structure is mostly localized in the nodal region for strains less than 11%. At higher strains, the deformation sets in all the struts and nodes of the hollow kagomé lattice. Owing to this two-stage deformation mechanism, the hollow Ni nanotube kagomé structure shows less bending and greater toughness than the solid Ni nanorod kagomé architecture.



In recent years, we have witnessed significant developments in the design of mechanical metamaterials with negative Poisson's ratio, negligible shear modulus, and negative compressibility.[1–4] These unusual properties of mechanical metamaterials have been exploited to design beautiful, intricate, robust, and scalable three-dimensional (3D) structures.[5–7] Recently, ultrathin and extraordinarily flexible sheets and hollow ceramic tubes have been synthesized.[8–13] These flexible structures have a wide range of applications in energy generation and storage (e.g., batteries and solar panels), flexible electronics and spintronics, self-actuated systems and stimuli-responsive sensing devices, and nanorobotics.

The field of metamaterials is still in its infancy, and there is very little theoretical understanding of mechanical properties of metamaterials.[14] The most common and the easiest way to study the mechanical behavior of mechanical metamaterials is Maxwell's constraint counting approach, which depends only on the number of internal degrees of freedom (DOF), $N_f$, and the number of internal mechanical constraints, $N_c$, in the system.[15] In the absence of stresses, there are three possibilities in the constraint-counting approach: (i) the system is under-constrained for $N_f > N_c$, (ii) the system is over-constrained when $N_f < N_c$, and (iii) the system is marginally stable when $N_f = N_c$. This approach provides a basic understanding of rigidity percolation and zero-energy modes in constraint-based materials. However, in real materials, there can be significant discrepancies between experiment and the constraint-counting approach because the latter leaves out an essential feature of real materials, namely, the existence of a hierarchy of length and energy scales associated with various DOFs.[2,16] Thus, it is quite conceivable that a system may be mechanically over-constrained and, therefore, rigid with respect to low-energy modes and respond compliantly with respect to high-energy modes if it is under-constrained.[17,18] The hierarchy of length and energy scales associated with internal DOFs in mechanical metamaterials has not yet been taken into account and, therefore, fundamental understanding of mechanical behavior under quasi-static and high strain-rate loading conditions is lacking.

In this paper, we describe deformation mechanical behavior of ultralight 3D kagomé structures consisting of hollow nickel (Ni) nanotubes and solid Ni nanorods.[19,20] Molecular dynamics (MD) simulations indicate the formation of $\frac{1}{6}[112]$ Shockley partial dislocations and twin formation in these systems. The kagomé structure made from solid nanorods shows deformation near both the nodes and beams at compressive strains above 5%. In the case of hollow nanotube architecture, most of the deformation is confined to the nodes of the kagomé structure for strains higher than 11%. We observe plastic buckling of solid and hollow architectures at 8% and 12.5% compression, respectively. Evidently, the hollow nanotube architecture can

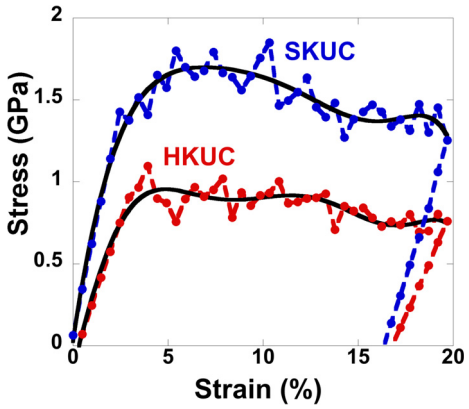


FIG. 1. Stress–strain curve of flat punch compression of SKUC and HKUC.

withstand much larger compression with very little deformation than the solid nanorod kagomé architecture.

We study deformation mechanisms in kagomé lattices (KLs) made from Ni nanorods and hollow tubes using MD simulations.[21–23] A $32.5 \times 32.5 \times 32.5\,\text{nm}^3$ KL is created by cutting eight cylinders from the Ni cubic lattice such that their axes are aligned along the four diagonals of the cubic lattice. The outer diameter of these cylinders is 10 nm, and they are either hollow (with a thickness of 2 nm) or solid. The length of struts in each KL is 25 nm, and the angle between them at the node is 45°. These KLs were subjected to uniaxial compression with a flat punch.[24] A fixed substrate of dimensions $52.8 \times 52.8 \times 2\,\text{nm}^3$ is placed at the top and bottom of the KLs. Figure S1 in the supplementary material shows a schematic of a KL. The details of the simulation setup for uniaxial flat punch compression are also given there.

Figure 1 shows stress–strain curves for the kagomé unit cell (KUC) made from solid Ni nanorods (SKUC) and hollow tubes (HKUC). The Young's moduli of SKUC and HKUC, computed from the elastic regime of stress–strain curves, are 54.8 GPa and 34.57 GPa, respectively. The SKUC has a higher Young's modulus because it has a higher density and, therefore, higher load-bearing capacity. The stress–strain curves also indicate that the yield point of HKUC is higher (3.9% strain) than that of SKUC (2.5% strain). These systems show differences not only in their Young's modulus and yield point but also in their response to compression after yielding. In the case of the SKUC, the load bearing capacity after the yield point decreases with an increasing strain. In contrast, the maximum load bearing capacity of HKUC remains constant up to 11% strain. The difference in stress–strain curves shows that the HKUC has higher strength and toughness.

We have also analyzed atomic stresses and plastic deformation around the yield point of these systems during compression and relaxation phases.[25,26] Plastic deformation is characterized by monitoring the nucleation and density of dislocations. We use an algorithm developed by Stukowaski *et al.* to identify different types of dislocations in a face-centered cubic (FCC) crystal and their Burgers vectors by computing the centro-symmetry parameter for each atom.[27,28]

We find nucleation of $\frac{1}{6}[112]$ Shockley partial and $\frac{1}{2}[110]$ dislocation loops on the $\langle 111 \rangle$ plane at the onset of deformation in SKUC. The dislocations are formed in interfacial regions between the KL and the flat punch and substrate. Partial dislocation loops propagate on the $\langle 111 \rangle$ plane from the top and bottom interfaces toward the nodal regions through the beams of the kagomé cell (see Fig. 2). Figure 2(a) shows dislocation nucleation near the substrate, and Fig. 2(b) shows the time step when the dislocation reaches the nodal region of the KL. Figure 2(b) also shows nucleation of new dislocation loops near the flat punch–SKUC interface. These dislocations also migrate to the

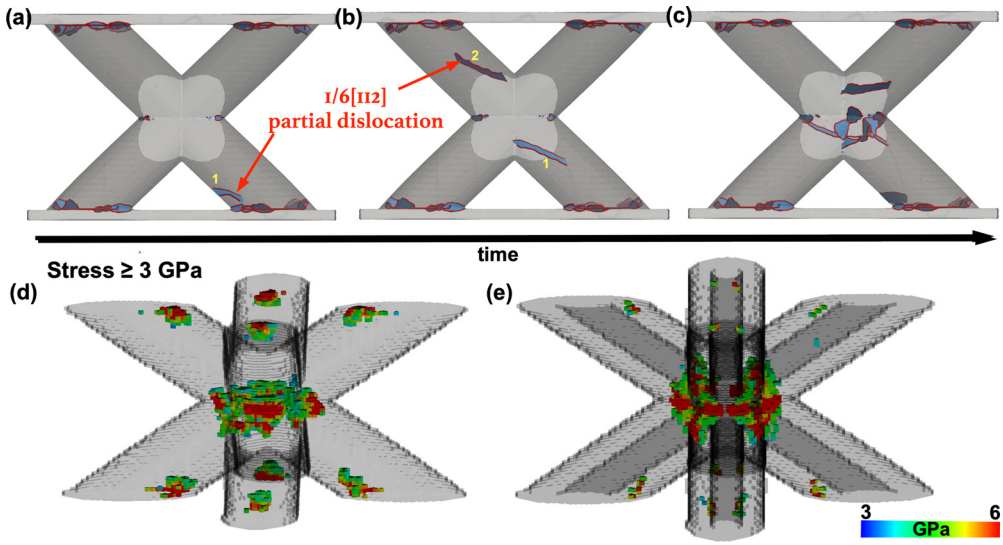


FIG. 2. (a)–(c) show plastic deformation of SKUC at the yield point. (a) shows the nucleation of a partial dislocation inside the SKUC near the substrate (marked as 1), which travels through the node of the SKUC cell on the (111) plane. (b) shows nucleation of another dislocation (marked as 2) near the flat punch–SKUC interface while dislocation 1 reaches the nodal area. This dislocation nucleation and annihilation processes continue and eventually we observe high dislocation density in the nodal region [shown in (c)]. (d) and (e) show regions where the stress is greater than 3 GPa inside the solid kagomé cell (d) and hollow kagomé cell (e) just before yielding.

nodal area of the kagomé cell. Dislocation loops interact with each other in the nodal region, and a large fraction of partial dislocation loops remains near the nodal region, see Fig. 2(c). A small fraction of dislocations leaves the system through the surface. The nodal area of the kagomé cell is a region of high dislocation density, and it acts as a source for dislocation nucleation along the interfaces. Since the dislocation density does not drop to zero, the system does not require higher stress for further plastic deformation; see Fig. S2(a). We also observe that the entire system of struts and the nodal region deforms during the onset of plastic deformation in the solid kagomé cell.

The deformation in a hollow kagomé cell is localized near the nodal area. Partial dislocation loops nucleate from the corners of the nodal area and migrate to interfaces of the kagomé cell with the flat punch and the substrate. The propagation of partial dislocation loops involves spiral motion on the ⟨111⟩ plane, which is also observed during the mechanical collapse of a single Ni nanotube subjected to flat punch compression (for details, see the supplementary material and movie S1). The spiral motion is caused by geometrical constraints on the HKUC because it does not have a direct path from the nodal region to the interfaces on the ⟨111⟩ plane. Therefore, the deformation is localized near the nodal area of the HKUC and dislocations do not reach the interface. Movies S2 and S3 in the supplementary material show plastic deformation and dislocation motion during yielding in these systems.

Figure S2(b) in the supplementary material shows dislocation density during yielding of the HKUC. The drop in the dislocation density is due to the annihilation of dislocation loops from the inner and outer walls of the kagomé cell. Note that the dislocation density does not vanish as it does in the case of the SKUC. Here again, the dislocation density is higher in the nodal region. In contrast to the solid kagomé cell, only the nodal region of the hollow kagomé cell deforms and the deformation in the struts is negligible.

The stress analysis before yielding indicates that the solid kagomé cell has a higher critical resolved shear stress near the nodal region and interfacial regions with the flat punch and substrate. In the case of a hollow kagomé cell, the maximum stress is near the nodal area. Figures 2(d) and 2(e) show regions of the SKUC and HKUC with stresses greater than 3 GPa. We have further quantified plastic deformations in these systems using local strain analysis during yielding (for details, see the supplementary material).[29–31] The analysis shows that deformation is localized near the nodal area of the HKUCs; see Fig. S3 in the supplementary material.

Figure 3 shows local deformation in a solid kagomé cell under compressive strains of 12% and 19%. Large regions of plastic deformation are observed at these high strains. The deformation is mostly inside the struts and nodal area of the kagomé cell. Several types of defects, such as twinned and slipped regions, are formed as shown in Figs. 3(b) and 3(d).

Figure 4 shows local deformation in the hollow kagomé cell under compressive strains of 11% and 19%. The stress–strain curve shows that HKUC undergoes a two-stage deformation mechanism. The maximum load-bearing capacity of the HKUC remains almost constant and there are localized regions of small deformation near the nodal area up to 11% strain. At higher strains, there is a drop in the stress–strain curve due to large deformations in the nodal region and also in the struts. For strains less than 11%, the maximum stress in the HKUC is near the nodal region and it shifts to the node and interfaces

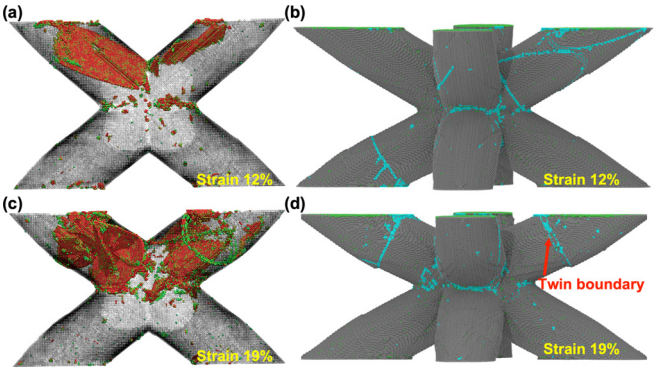


**FIG. 3.** Local deformation analysis shows regions of plastic deformation in SKUC at 12% and 19% strain. (a) and (c) show internal regions with local deformation parameter, $D^2_{min}$, greater than 0.25, and (b) and (d) show twin boundaries at the outer surface of the SKUC.

at higher compressive strains. Movies S4 and S5 in the supplementary material show local strain analysis for SKUC and HKUC as a function of the applied strain. Figure S4 shows dislocation densities inside the SKUC and HKUC as a function of the applied strain, which again shows that SKUC has a higher dislocation density even though the mass per unit volume is the same for both systems, i.e., nickel density at the beginning of simulation.

Stretching and bending are the dominant deformation mechanisms in hierarchical metamaterials.[14,32] Schaedler *et al.* have observed bending in flat-punch compression of a kagomé lattice made from poly-crystalline Ni.[12] We observe bending of struts in response to compressive load on kagomé cells. Figure 5 shows bending of beams as a function of the applied strain. The solid kagomé cell shows higher bending than the hollow kagomé cell. The deformation in the hollow kagomé cell is localized near the nodal region up to 11% strain. Smaller bending and plastic deformation indicate that the hollow

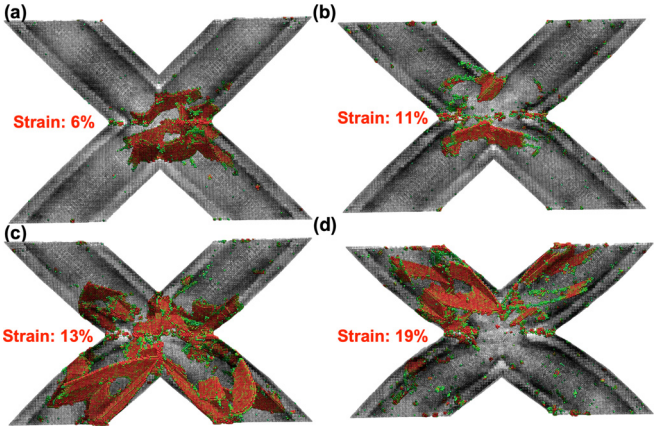


**FIG. 4.** Local deformation analysis showing regions of plastic deformation in HKUC as a function of the applied strain. Here, up to 11% strain deformation is localized near the nodal area of HKUC (a) and (b) beyond which both the node and struts deform (c) and (d).

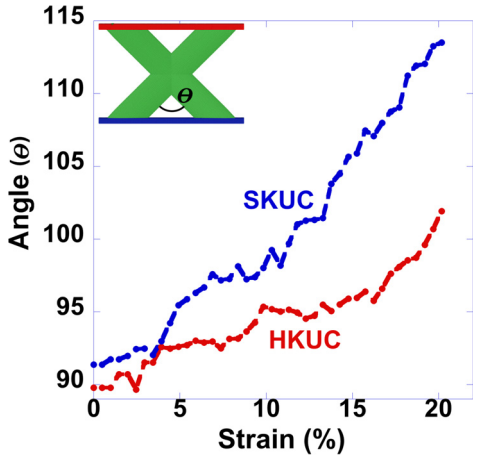


**FIG. 5.** Angle $\theta$ between the struts at the node varies with the applied strain on SKUC and HKUC. In the case of SKUC, the angle $\theta$ increases constantly with applied strain, however, in the case of HKUC, it shows rapid increase above 11% strain.

kagomé cell has higher strength and toughness than the solid kagomé cell.

In summary, we observe that the hollow kagomé unit cell (3.9% strain) has a higher yield point than a solid kagomé unit cell (2.5% strain). HKUCs show a two-stage deformation process: for strains less than 11%, the deformation is localized near the nodal region; above 11% strain, deformation sets in all the struts and nodes. Owing to this two-stage deformation mechanism, HKUCs show less bending and higher toughness than SKUCs.

We have also studied the effect of uniaxial compression on a large KL of dimensions $210 \times 140 \times 70\,\text{nm}^3$, which is made from hollow KUC and consists of $\sim 30 \times 10^6$ atoms. This larger KL lattice also shows a unique deformation mechanism, e.g., localized deformation in the middle kagomé cells, but very little deformations in the rest of the system at strains as high as 15%. The details of the effect uniaxial compression on the larger KL are given in the supplementary material.

See the supplementary material for the simulation details, description of interaction potential used in the simulation, details of local deformation analysis, analysis of dislocation density inside SKUC and HKUC during yielding, uniaxial deformation hollow tube, and uniaxial compression of the large hollow kagomé lattice.

This work was supported by the National Science Foundation, Future Manufacturing Program, Award NSF 2036359. This research was partly supported by Aurora Early Science programs and used resources of the Argonne Leadership Computing Facility, which is a DOE Office of Science User Facility supported under Contract DE-AC02-06CH11357, and Center for Integrated Nanotechnologies at Sandia National Laboratories, which is a multi-mission laboratory managed and operated by National Technology and Engineering Solutions of Sandia, LLC., a wholly owned subsidiary of Honeywell International, Inc., for the U.S. DOE's National Nuclear Security Administration under contract DE-NA-0003525. Computations were performed at the Argonne Leadership Computing Facility under the DOE INCITE and Aurora Early Science programs and at the Center for Advanced Research Computing of the University of Southern California.

## DATA AVAILABILITY

The data that support the findings of this study are available from the corresponding author upon reasonable request.

## REFERENCES

[1]X. Yu, J. Zhou, H. Liang, Z. Jiang, and L. Wu, Prog. Mater. Sci. **94**, 114 (2018).
[2]R. Lakes, Nature **361**(6412), 511 (1993).
[3]N. A. Fleck, V. S. Deshpande, and M. F. Ashby, Proc. R. Soc. A **466**(2121), 2495 (2010).
[4]F. Libonati and M. J. Buehler, Adv. Eng. Mater. **19**(5), 1600787 (2017).
[5]L. R. Meza, G. P. Phlipot, C. M. Portela, A. Maggi, L. C. Montemayor, A. Comella, D. M. Kochmann, and J. R. Greer, Acta Mater. **140**, 424 (2017).
[6]Y. Jiang and Q. Wang, Sci. Rep. **6**, 34147 (2016).
[7]Z. Qin, G. S. Jung, M. J. Kang, and M. J. Buehler, Sci. Adv. **3**(1), e1601536 (2017).
[8]A. J. Jacobsen, W. B. Carter, and S. Nutt, Acta Mater. **55**(20), 6724 (2007).
[9]L. R. Meza, S. Das, and J. R. Greer, Science **345**(6202), 1322 (2014).
[10]L. C. Montemayor, L. R. Meza, and J. R. Greer, Adv. Eng. Mater. **16**(2), 184 (2014).
[11]L. C. Montemayor and J. R. Greer, J. Appl. Mech. **82**(7), 071012 (2015).
[12]T. A. Schaedler, A. J. Jacobsen, A. Torrents, A. E. Sorensen, J. Lian, J. R. Greer, L. Valdevit, and W. B. Carter, Science **334**(6058), 962 (2011).
[13]J. Lian, D. Jang, L. Valdevit, T. A. Schaedler, A. J. Jacobsen, W. B. Carter, and J. R. Greer, Nano Lett. **11**(10), 4118 (2011).
[14]L. J. Gibson and M. F. Ashby, *Cellular Solids: Structure and Properties* (Cambridge University Press, Cambridge, 1999).
[15]J. C. Maxwell, London, Edinburgh, Dublin Philos. Mag. J. Sci. **27**(182), 294 (1864).
[16]L. R. Meza, A. J. Zelhofer, N. Clarke, A. J. Mateos, D. M. Kochmann, and J. R. Greer, Proc. Natl. Acad. Sci. **112**(37), 11502 (2015).
[17]J. C. Wallach and L. J. Gibson, Int. J. Solids Struct. **38**(40), 7181 (2001).
[18]Y. H. Zhang, X. M. Qiu, and D. N. Fang, Int. J. Solids Struct. **45**(13), 3751 (2008).
[19]N. G. W. Haydn, Philos. Trans. R. Soc. A **364**(1838), 31 (2006).
[20]K. Wei, Q. Yang, B. Ling, H. Xie, Z. Qu, and D. Fang, Extreme Mech. Lett. **23**, 41 (2018).
[21]S. Plimpton, J. Comput. Phys. **117**(1), 1 (1995).
[22]Y. Li, A. Goyal, A. Chernatynskiy, J. S. Jayashankar, M. C. Kautzky, S. B. Sinnott, and S. R. Phillpot, Mater. Sci. Eng. A **651**, 346 (2016).
[23]S. S. Hayat, M. A. Ortigoza, M. A. Choudhry, and T. S. Rahman, Phys. Rev. B **82**(8), 085405 (2010).
[24]A. M. Dongare, A. M. Rajendran, B. LaMattina, M. A. Zikry, and D. W. Brenner, Comput. Mater. Sci. **49**(2), 260 (2010).
[25]A. P. Thompson, S. J. Plimpton, and W. Mattson, J. Chem. Phys. **131**(15), 154107 (2009).
[26]K. Mackenchery, R. R. Valisetty, R. R. Namburu, A. Stukowski, A. M. Rajendran, and A. M. Dongare, J. Appl. Phys. **119**(4), 044301 (2016).
[27]H. Tsuzuki, P. S. Branicio, and J. P. Rino, Comput. Phys. Commun. **177**(6), 518 (2007).
[28]A. Stukowski and K. Albe, Modell. Simul. Mater. Sci. Eng. **18**(8), 085001 (2010).
[29]P. Rajak, R. K. Kalia, A. Nakano, and P. Vashishta, ACS Nano **12**(9), 9005 (2018).
[30]E. D. Cubuk, R. J. S. Ivancic, S. S. Schoenholz, D. J. Strickland, A. Basu, Z. S. Davidson, J. Fontaine, J. L. Hor, Y. R. Huang, Y. Jiang *et al.*, Science **358**(6366), 1033 (2017).
[31]E. D. Cubuk, S. S. Schoenholz, J. M. Rieser, B. D. Malone, J. Rottler, D. J. Durian, E. Kaxiras, and A. J. Liu, Phys. Rev. Lett. **114**(10), 108001 (2015).
[32]V. S. Deshpande, M. F. Ashby, and N. A. Fleck, Acta Mater. **49**(6), 1035 (2001).